UNIVERSITY OF OKLAHOMA

GRADUATE COLLEGE

THE EFFECT OF PORE WATER EVAPORATION ON TRANSPORT OF CAFFEINE, PROPRANOLOL AND CIPROFLOXACIN: A SAND COLUMN STUDY AND MODEL SIMULATION

A THESIS

SUBMITTED TO THE GRADUATE FACULTY

in partial fulfillment of the requirements for the

Degree of

MASTER OF SCIENCE IN ENVIRONMENTAL ENGINEERING

By

HAYLEY J. NORMILE
Norman, Oklahoma
2016

Downloaded from SHAREOK. Persistent Handle URL: https://hdl.handle.net/11244/45152

THE EFFECT OF PORE WATER EVAPORATION ON TRANSPORT OF CAFFEINE, PROPRANOLOL AND CIPROFLOXACIN: A SAND COLUMN STUDY AND MODEL SIMULATION

A THESIS APPROVED FOR THE
SCHOOL OF CIVIL ENGINEERING AND ENVIRONMENTAL SCIENCE

BY

_____
Dr. Tohren Kibbey, Chair

_____
Dr. David Sabatini

_____
Dr. Mark Nanny

© Copyright by HAYLEY J. NORMILE 2016
All Rights Reserved.

Acknowledgements

This material is based upon work supported by the National Science Foundation under Grant No. 1336083.

Table of Contents

Acknowledgements iv
Table of Contents v
List of Tables vi
List of Figures vii
Abstract viii
Chapter 1. Introduction 1
Chapter 2. Experimental 3
2.1 Chemical compounds 3
2.2 Model development 4
2.3 Materials 9
2.4 Detection methods 10
2.5 Procedure 10
Chapter 3. Results & Discussion 13
3.1 Saturated experiments: characterizing sorption behavior 13
3.2 Unsaturated experiments: observing the effect of evaporation and dissolution 14
3.3 Desorption-only model inputs 15
3.4 Fluorescein 15
3.5 Sulforhodamine B 17
3.6 Caffeine 18
3.7 Propranolol 20
3.8 Ciprofloxacin 22
3.9 Elution curve centroid analysis 24
3.10 Discussion 27
3.11 Solid precipitate analysis 28
3.12 Further exploration of dissolution effect 29
Chapter 4. Environmental Implications 31
References 33

List of Tables

Table 1: Chemical properties of select pharmaceuticals and tracers 3
Table 2: Experimental data from saturated experiments to characterize adsorption of the pharmaceuticals and tracers used in this study 14
Table 3: Elution curve centroids for experimental and model results 25
Table 4: Molecular coating depth 29

List of Figures

Figure 1: Simulated distributions of C and q for a saturated column at equilibrium (black, blue lines), and an unsaturated column after imbibed from left to right with reference solution (red, green lines)..... 7
Figure 2: Sand column distribution of tracer dye (sulforhodamine B) in a) saturated experiment and b) unsaturated experiment. 7
Figure 3: Simulated elution curves for the a) saturated case and b) unsaturated case. The dotted line indicates the breakthrough of 0.5 C/C_O occurring at PV = 1, which is true for R_f = 1.0, i.e., the case of no adsorption..... 9
Figure 4: Sand column undergoing imbibition over time. Solution is flowed from bottom to top. Note: top area of the column is dark due to shadow, not wetted with solution..... 12
Figure 5: Elution curves for saturated experiments 13
Figure 6: Elution curves for unsaturated experiments 15
Figure 7: Fluorescein elution curves for a) saturated and b) unsaturated experiments. Dotted line simulates the desorption-only result. 16
Figure 8: Sulforhodamine B elution curves for a) saturated and b) unsaturated experiments. Dotted line simulates the desorption-only result. 18
Figure 9: Caffeine elution curves for a) saturated and b) unsaturated experiments. Dotted line simulates the desorption-only result. 20
Figure 10: Propranolol elution curves for a) saturated and b) unsaturated experiments at pH 5 and 10. Dotted line simulates the desorption-only result. 22
Figure 11: Ciprofloxacin elution curves for a) saturated and b) unsaturated experiments at pH 3 and 10. Dotted line simulates the desorption-only result. 24
Figure 12: The relationship between the centroid ratio (X_{EXP}/X_{MOD}) and the concentration normalized to the compound solubility (C_O/S), on log-log scale. 26
Figure 13: The relationship between the centroid ratio (X_{EXP}/X_{MOD}) and the experimentally-determined distribution coefficient (K_d), on log-log scale. 27
Figure 14: The relationship between the centroid ratio (X_{EXP}/X_{MOD}) and the concentration normalized to the compound solubility (C_O/S), on log-log scale, for additional sulforhodamine B experiments. 30

Abstract

The purpose of this study was to explore the transport of selected pharmaceuticals under saturated and unsaturated conditions, simulating environmental processes of evaporation and flooding. Caffeine (a stimulant), propranolol (a beta blocker), and ciprofloxacin (an antibiotic), were used in multiple sand column experiments that examined sorption behavior under two conditions: 1) standard, completely saturated sand column experiments, and 2) saturated sand column experiments where intermediate steps of partial drainage and complete pore water evaporation were introduced before the final flushing stage. The experimental flushing-out breakthrough curves, or elution curves, were compared to simulated elution curves. The model employed in this study was developed using a one-dimensional transport equation accounting for advection, adsorption, and dispersion. Differences between the experimental and simulated curves were attributed to the effects of rate-limited dissolution. Results suggest that dissolution hinders the removal of each pharmaceutical during flushing. The effect of dissolution is explored as it relates to the retention of mass in the column. Findings suggest that dissolution affects the transport of a compound based on the relationship between the concentration and solubility values: a ratio of C_O/S close to 1 shows little dissolution effect, whereas C_O/S ratios much less than 1 show greater dissolution effect.

Chapter 1. Introduction

As emerging organic contaminants, pharmaceutical compounds play an increasingly important role in contamination of the environment. These compounds are present in waste produced by humans, animals, hospitals, and industrial effluents, and can enter the environment via landfill leachate, leaks in sewage and wastewater systems, surface runoff, and illegal dumping.[1,2] Even treated wastewater effluent, though compliant with regulatory levels, can contain low concentrations of pharmaceuticals.[3] Consequent contamination occurs in surface water, groundwater, and the subsurface, and has been detected in several countries.[4,5,6,7,8] Water sources and wastewater effluents have been found to contain up to 0.03 $\mu g\ L^{-1}$ ciprofloxacin antibiotic, 0.59 $\mu g\ L^{-1}$ propranolol beta blocker, and 15.9 $\mu g\ L^{-1}$ caffeine stimulant.[9,10,11] These and other pharmaceutical contaminants can cause harm to human and environmental health, specifically the potential of subsurface antibiotic contamination to cause antibiotic resistance of bacteria[12,13], and the cytotoxicity of beta blockers to fish hepatocytes.[14]

Some techniques for removal and disposal of pharmaceutical-contaminated flows include: sand filtration[15], graphene adsorption reactors[15], biologically active carbon filtration[3], sludge stabilization for sludge landspreading[16], constructed wetlands[17], and riverbank filtration.[18,19] These techniques rely on sorption, among other processes, to remove contaminants. Sorption data via sand column experiments has been published for propranolol[20], caffeine[2,20], and ciprofloxacin[21], but not for the unsaturated conditions explored in this study.

The purpose of this study was to use sand column experiments under varying saturations to simulate the effects of pore water evaporation on the transport of select pharmaceuticals. Evaporation of the column was introduced as an intermediate step in the sand column experiment, between flushing with the compound solution, and flushing out the compound with a reference solution. The effect of evaporation was quantified by comparing experimental flushing-out breakthrough curves, or elution curves, to simulated elution curves via centroids. The simulations are designed to model transport via adsorption/desorption, advection, and dispersion during the saturation and flushing processes, allowing for interpretation of the effects of rate limited dissolution on transport based on observed differences between simulations and experiments.

Chapter 2. Experimental

2.1 Chemical compounds

Three pharmaceutical compounds were used for sand column experiments: caffeine, a stimulant; propranolol, a beta blocker; ciprofloxacin, an antibiotic (Table 1). Two fluorescent dyes, fluorescein and sulforhodamine B, were selected to act as model low-adsorption compounds (Table 1). The five compounds were selected to cover a range of sorption behaviors and to be easily detected via UV-spectrometry for real-time analyses. Fluorescein (Sigma-Aldrich) and sulforhodamine B (as sodium salt, Sigma-Aldrich) acted as near-conservative tracers for preliminary experiments. Caffeine (Sigma-Aldrich) has relatively low adsorption. Propranolol (as propranolol-HCl, Sigma-Aldrich) has pH-dependent adsorption behavior. Ciprofloxacin (Sigma-Aldrich) exhibits zwitterionic behavior and has highly pH-dependent adsorption. Stock solutions used degassed Nano-pure water, and pH was controlled with HCl and NaOH addition. All solutions had an ionic strength of 0.01 M via $CaCl_2$ dihydrate (Carolina Biological Supply Company). For each experiment, a reference solution was made with identical ionic strength and pH as the compound solution.

Table 1: Chemical properties of select pharmaceuticals and tracers

Compound	pK_a	MM ($g\ mol^{-1}$)	pH	Solubility ($mg\ L^{-1}$)	log K_{ow}
Fluorescein[22,23]	5.1	376.2	-	25,000	-0.39
Sulforhodamine B[22]	<1.5	604.7	-	70,000	-2.02
Caffeine[20,6]	0.60[a]	194.2	-	21,600	-0.07[b]

Compound	pK_a	MM ($g\ mol^{-1}$)	pH	Solubility ($mg\ L^{-1}$)	log K_{ow}
Propranolol[24]	9.53[a]	259.4	5 10	62.2[d] 245.8[d]	0.78[c] 3.48[b]
Ciprofloxacin[24,25]	6.16[a] 8.62[a]	331.4	3 10	89,232[d] 1,542[d]	-1.69[c] -1.08[b]

[a] Value at 0.15 M Ionic strength[25]
[b] Octanol-water partitioning coefficient of neutral species[25]
[c] Octanol-water partitioning coefficient of cationic species[25]
[d] Value at 0.15 M Ionic strength, calculated from intrinsic solubility[25]

2.2 Model development

A model was developed for simulating the desorption process in a sand column under two scenarios: 1) saturated, and 2) unsaturated. The **saturated** scenario includes the following steps: the column is flushed with a solution at constant concentration (C_o) until equilibrium adsorption is reached (i.e., outlet concentration equals C_o); the column is flushed with a reference solution until all mass is removed from the column (i.e., outlet concentration equals zero). In this scenario, the compound can be adsorbed to the column media, or in solution. The **unsaturated** scenario includes the following steps: the column is flushed with a solution at C_o until equilibrium adsorption is reached; the column is drained to a set saturation (e.g., 40%); the column pore water is evaporated until contents are dried; the column is imbibed with reference solution (filling the dry cell to 100% saturation); the column is flushed until all mass is removed from the column. In this scenario, the compound is at first adsorbed to column media and in solution. As evaporation takes place, the pore water remaining in the column dries, and the compound in solution becomes more concentrated. Once the column is completely dried, it is assumed that all mass remaining is adsorbed to the sand surface as solid

precipitate. As the column is re-saturated, the solid adsorbed will dissolve into solution and desorb from the sand surface.

The model simulates the movement of mass in the column using the one-dimensional saturated transport equation, which describes the processes of diffusion and dispersion, adsorption, and advection:[26]

$$\frac{\partial C}{\partial t} = D\frac{\partial^2 C}{\partial x^2} - v\frac{\partial C}{\partial x} - \frac{M}{V}\frac{\partial q}{\partial t} \quad (1)$$

Where D is the diffusion/dispersion coefficient dominated by dispersion via $D = \alpha \cdot v$, where α is dispersivity (m), M is the mass of sand in the column, V is the pore volume of the column, and v is the pore water velocity (m s^{-1}). The adsorption/desorption rate, $\frac{\partial q}{\partial t}$, of mass to sand in the column is modeled by rate-limited linear adsorption:

$$\frac{\partial q_i}{\partial t} = k_{des}(K_d C_i - q_i) \quad (2)$$

Where k_{des} is the desorption rate (s^{-1}), K_d is the distribution coefficient (L kg^{-1}), C_i is the aqueous concentration (mg L^{-1}), and q_i is the mass adsorbed to the sand surface (mg kg^{-1}). Equations 1 and 2 are transformed to finite difference form, and combined to produce Equation 5:

$$\frac{C_i^{n+1} - C_i^n}{\Delta t} = \frac{D}{\Delta x^2}[C_{i+1}^{n+1} - 2C_i^{n+1} + C_{i-1}^{n+1}] - \frac{M}{V}\frac{k_{des}}{\Delta t}(K_d C_i^{n+1} - q_i^{n+1}) - \frac{v}{\Delta x}[C_i^{n+1} - C_{i-1}^{n+1}] \quad (3)$$

$$\frac{q_i^{n+1} - q_i^n}{\Delta t} = k_{des}(K_d C_i^{n+1} - q_i^{n+1}) \quad (4)$$

$$C_{i+1}^{n+1}\left[-\frac{\Delta t}{\Delta x^2}D\right]+C_i^{n+1}\left[1+2\frac{\Delta t}{\Delta x^2}D+\frac{M}{V}k_{des}K_d(1-r_3)-\frac{\Delta t}{\Delta x}v\right] \quad (5)$$

$$+C_{i-1}^{n+1}\left[-\frac{\Delta t}{\Delta x^2}D+\frac{\Delta t}{\Delta x}v\right]=C_i^n+q_i^n\left[\frac{M}{V}\frac{r_3}{\Delta t}\right]$$

Where r_3 is defined as $\frac{k_{des}\Delta t}{1+k_{des}\Delta t}$. Equation 5 is used in the program to simulate the diffusion, adsorption, and advection of mass being flushed from the column in both the saturated and unsaturated cases.

Before flushing with a reference solution, the initial distribution of mass in the column is determined. For the **saturated** case, the column begins in equilibrium with evenly distributed mass in the adsorbed state, q, and aqueous state, C, according to the distribution coefficient (Figs. 1, 2a). The distribution coefficient, K_d, is calculated by experimentally-determined values of the retardation factor, R_f:

$$R_f = 1.0 + \frac{\rho_b}{n}K_d \quad (6)$$

Where R_f represents the number of pore volumes required to remove all mass from the column during flushing, ρ_b is the bulk density (kg m^{-3}), and n is the packing porosity. An R_f of 1.0 means that no mass is adsorbed to sand. R_f increases as the extent of adsorption increases. R_f varies slightly with small differences in packing porosity. For the **unsaturated** case, the column begins with mass distributed along the column after imbibition (i.e., starting from dry and filling with reference solution until reaching 100% saturation) (Figs. 1, 2b). In Figure 1, the column is filled from left to right, and the mass is distributed more densely at the right end of the column. An illustration of this distribution is shown using a visible tracer dye sulforhodamine B, where the column is filled from bottom to top (Fig. 2).

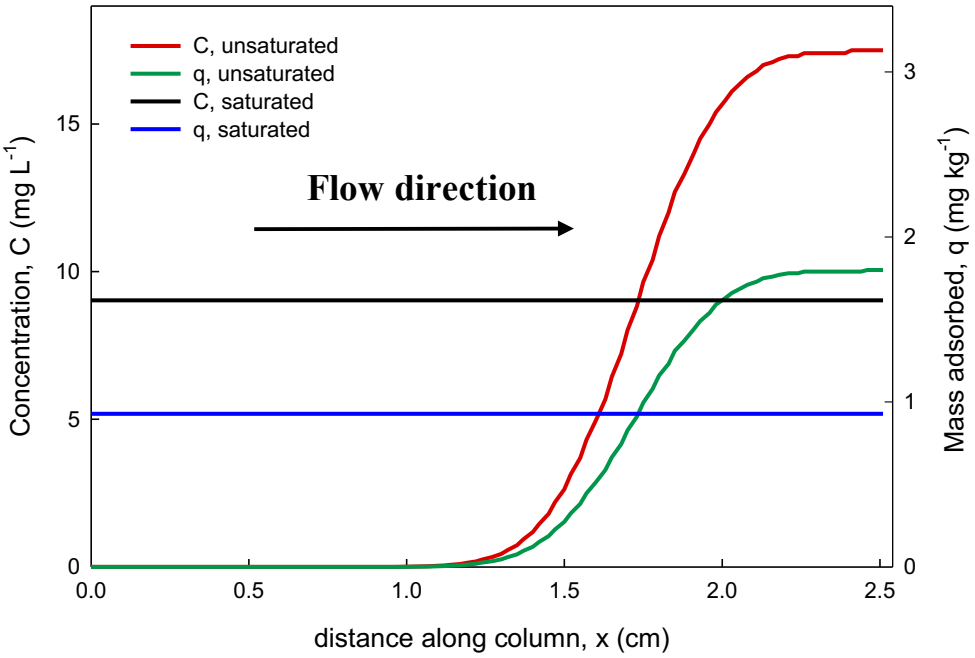


Figure 1: Simulated distributions of *C* and *q* for a saturated column at equilibrium (black, blue lines), and an unsaturated column after imbibed from left to right with reference solution (red, green lines).

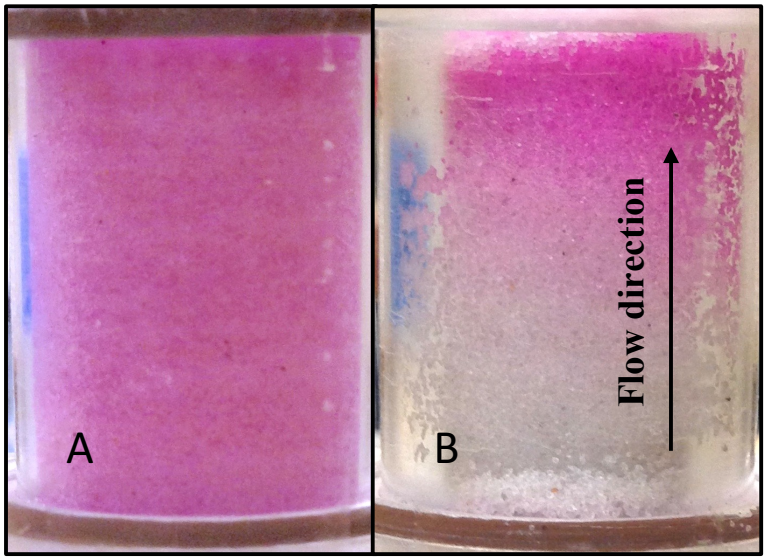


Figure 2: Sand column distribution of tracer dye (sulforhodamine B) in a) saturated experiment and b) unsaturated experiment.

After the initial distribution is determined, the program simulates the column being flushed with reference solution until all mass is removed. The **saturated** case begins with evenly distributed mass in the column, and produces typical s-shaped elution curves (Fig. 3a). The area below each curve corresponds to its R_f value. The **unsaturated** case begins with the uneven distribution of mass in the column, and produces elution curves of varying shape (Fig. 3b). R_f values closer to 1.0 produce elution curves with a high initial peak in outlet concentration, whereas R_f values much greater than 1.0 produce elution curves with longer tails and no peak in initial outlet concentration. An interesting observation from the simulations in Figure 3b is that compounds that exhibit low adsorption (low R_f) leave the column at concentrations greater than the initial concentration (i.e., $C/C_O > 1$) as a result of the resaturation process, where dried mass is dissolved and swept along in the imbibing front, concentrating at the column outlet (Figs. 1, 2).

A process not included in the simulation is dissolution. This is important for unsaturated experiments, where the evaporation step forces the remaining mass adsorbed and in solution to form solids as precipitates on the sand surface. During the imbibing step, immediate dissolution is assumed, producing distributions of Figure 1. However, if dissolution is rate-limited, it may have a bigger impact on the distribution of C and q along the column, by inhibiting the mass from being so easily removed during flushing. Since initial distribution of C and q in the column is not known in experiments, the elution curves are used to observe the effect of dissolution.

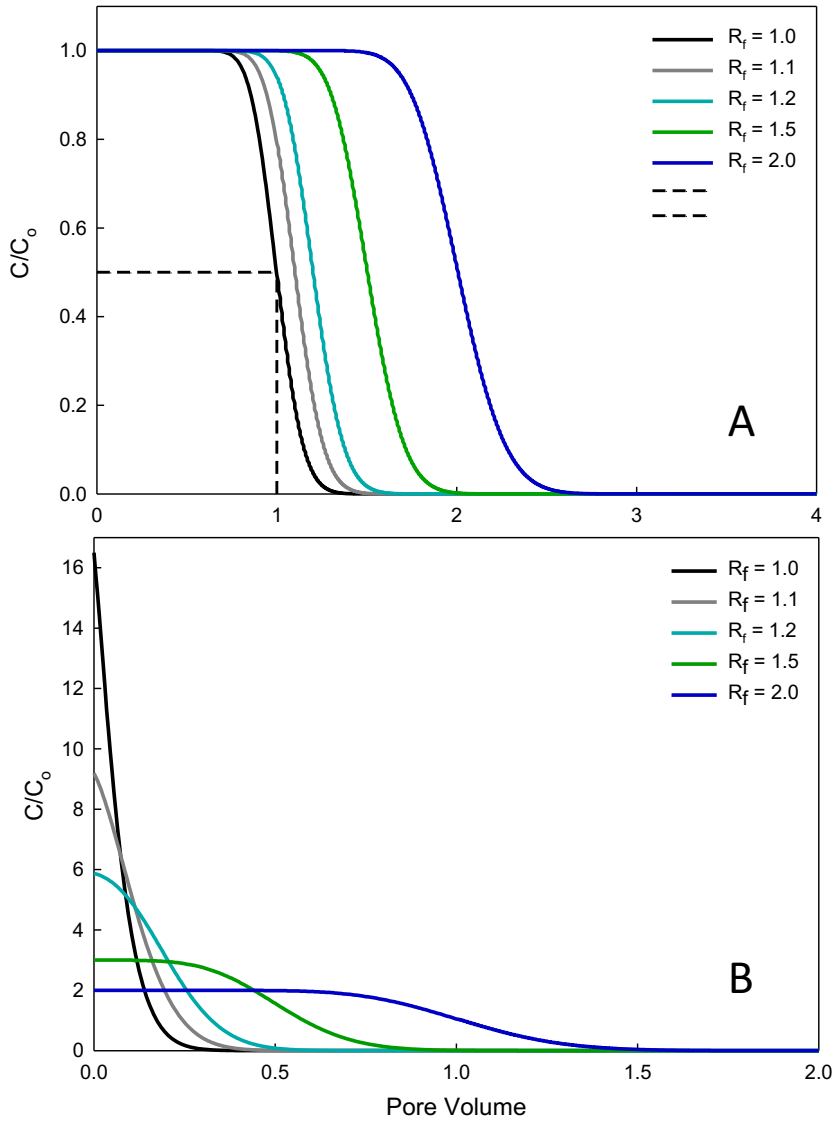


Figure 3: Simulated elution curves for the a) saturated case and b) unsaturated case. The dotted line indicates the breakthrough of 0.5 C/C_O occurring at PV = 1, which is true for R_f = 1.0, i.e., the case of no adsorption.

2.3 Materials

All experiments used a cylindrical vertical column measuring 2.54 cm (1 inch) in height, 1.91 cm (0.75 inch) in diameter, and 6.72 cm^3 in cell volume. The column was packed with US Silica (Berkeley Spring, WV) F-65 Ottawa fine sand with an average packed porosity of 0.37. Before packing, the sand was rinsed with deionized

water several times and dried in an oven at 110 degrees Celsius. Paper filters (Ahlstrom qualitative filter papers, 1.5 μm pore size) and mesh screens (stainless steel mesh #40, type 304, 0.38 mm, 36% open area) were held in place at both ends of the column by an O-ring for a water-tight fit. During drainage and evaporation, the paper filter on the bottom of the column was replaced by a Teflon membrane (Tisch Scientific, PTFE membrane filter, 0.22 μm pore size) to allow the passage of air through the cell.

2.4 Detection methods

Outlet flow from the sand column was analyzed with UV spectrophotometric detection, using methods described in detail by Chen and Kibbey.[27] After leaving the column, effluent solution entered an optical cell fitted with a fiber optic spectrometer (Ocean Optics, Inc.) and a deuterium light source (Mikropack) attached with a fixed optical path length. This measured the absorbance spectrum of the outlet flow on a set time-interval (either 1-sec or 10-sec) throughout the experiment. A fitting program was used to analyze the measured absorbance against known standard spectrum curves. Standards were measured for each compound (multiple standards for compounds with pH-dependent spectra) and sand fines. At the end of each experiment, the sand column contents were collected and stored with a known amount of an extraction solvent of methanol or acetonitrile. After 12-24 hours, the supernatant was collected and read in by UV/Visible spectrophotometer (Shimadzu UV-1601).

2.5 Procedure

Saturated experiments were conducted with the column at complete saturation. The column was flushed with different solutions using a 50-mL syringe pump (KD Scientific) at a rate of 0.50 mL min^{-1} (0.50 cm min^{-1} pore water velocity). The column

was first flushed with a reference solution for at least five (5) pore volumes (PVs) in order to stabilize the sand column pH and flush out sand fines. Immediately after, the column was flushed with the compound solution until the outlet concentration reached and plateaued at the inlet stock concentration. Finally, the column was flushed with the reference solution until the outlet concentration reached a plateau at approximately zero. For saturated experiments, the cell was oriented vertically, with inlet flow entering the top of the column, and outlet flow exiting the bottom of the column.

Unsaturated experiments were conducted with the column at various levels of saturation. The steps included flushing, draining, evaporation, and re-flushing (including re-saturating the column dried from evaporation). First, the column was flushed with the reference solution and compound stock solution as described in the saturated procedure. For this portion, the cell was oriented vertically, with inlet flow entering the top of the column, and outlet flow exiting the bottom of the column. Then, the cell was attached to a system with applied air pressure at the top end of the column, and an outlet tube to the bottom of the column, connected to a water height pressure transducer. For this drainage step, the top filter was changed to a Teflon membrane, and the bottom filter remained the same paper filter used during flushing. As air pressure was applied to the column, the pore water drained into the outlet tube. The transducer measurement was used to track saturation within the cell during drainage. For drainage, the column began at full saturation, and used a ramped air pressure flow of until the cell reached approximately 40% saturation, taking approx. 45 minutes. At this point, the cell was inverted, and the now-top cap on the column was removed in order to act as a vent, and air was forced through the column at constant inlet pressure

(~2 psi) to completely evaporate the sand contents. The process of evaporating from 40% to 0% saturation was recorded by measuring the column weight over time via an electronic balance (Ohaus). Evaporation lasted between six (6) and (8) hours, and air flow continued for another four (4) to six (6) hours to ensure complete dryness. After evaporation, the dry cell was inverted and both filters were replaced with paper filters, then resaturated by flowing the reference solution through the bottom of the column, allowing the solution to fill all the voids and the pore air to evacuate through the open top of the column (Fig. 4). Once filled, the column top was attached, and the flow was resumed. The reference solution was then flushed through the now-saturated column until all of the compound remaining in the column was flushed out.

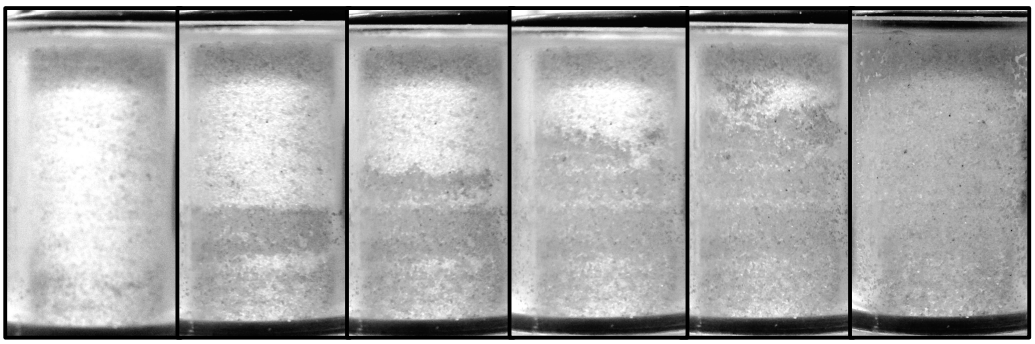


Figure 4: Sand column undergoing imbibition over time. Solution is flowed from bottom to top. Note: top area of the column is dark due to shadow, not wetted with solution.

Chapter 3. Results & Discussion

3.1 Saturated experiments: characterizing sorption behavior

Figure 5 shows the flushing-out breakthrough curves, or elution curves, for standard, saturated experiments. These elution curves have the same general shape, with the curvature varying slightly from experiment to experiment. Fluorescein is not shown here because its curve was not as clearly defined as the alternative tracer, sulforhodamine B. The level of adsorption for each compound, as measured by R_f and K_d, is reported in Table 2. The compounds can be ranked from lowest to highest adsorption by R_f value: fluorescein < sulforhodamine B < propranolol (pH 10) ≈ caffeine < ciprofloxacin (pH 10) < propranolol (pH 5) < ciprofloxacin (pH 3). As shown in Figure 5 and Table 2, the bulk of experiments resulted in R_f values between 1 and 2. Only the low pH ciprofloxacin experiment had a substantially higher R_f compared to the other compounds.

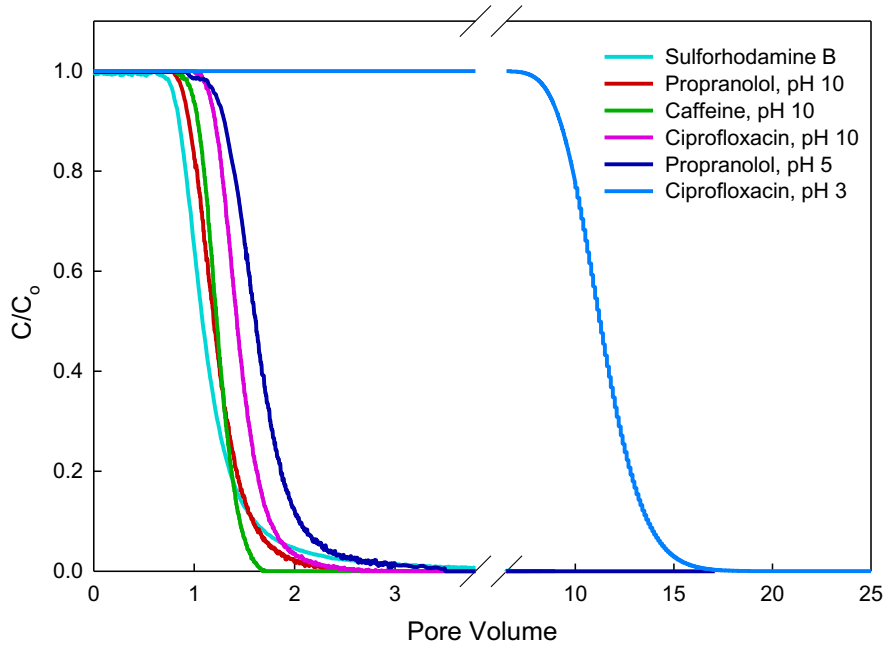


Figure 5: Elution curves for saturated experiments

Table 2: Experimental data from saturated experiments to characterize adsorption of the pharmaceuticals and tracers used in this study

Compound	C_O (mg L^{-1})	pH	R_f	K_d (L kg^{-1})
Fluorescein	1.48	10	1.171	0.038
Sulforhodamine B	41.6	3	1.194	0.043
Caffeine	27.0	10	1.245	0.054
Propranolol	10.0	5	1.657	0.146
	10.0	10	1.242	0.054
Ciprofloxacin	12.5	3	11.122	2.243
	10.3	10	1.464	0.103

3.2 Unsaturated experiments: observing the effect of evaporation and dissolution

Figure 6 shows the elution curves for all unsaturated experiments. These curves are created by imbibing the dried cell and then flushing, and vary in range and shape. Sulforhodamine B and propranolol (pH 10) show similar behavior, and are flushed out relatively quickly. Caffeine, ciprofloxacin (pH 10), and propranolol (pH 5) are more delayed, with lower peak outlet concentrations and more curvature. Lastly, ciprofloxacin (pH 3) experiences the most delayed removal of all compound/pH conditions.

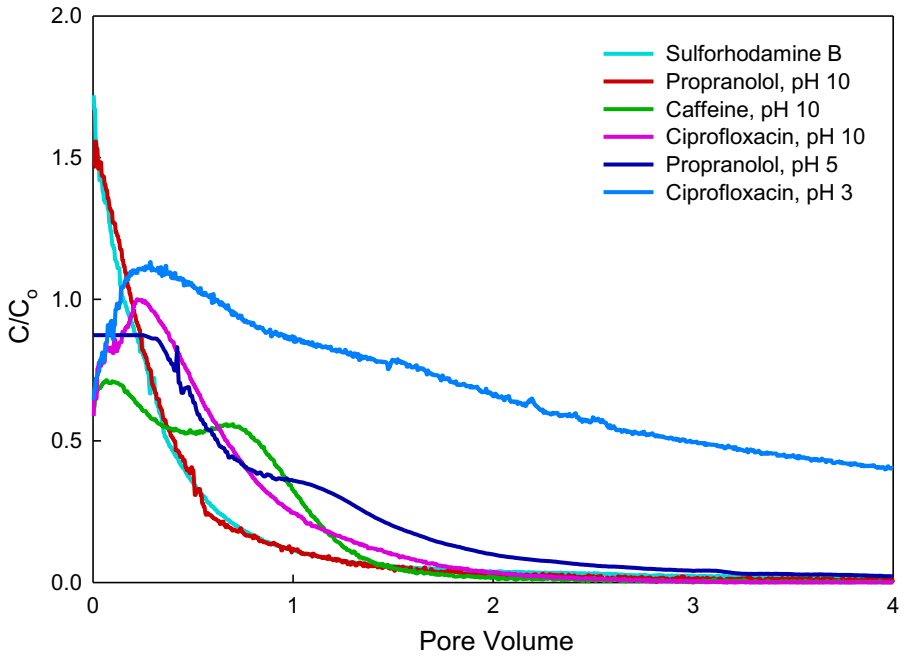


Figure 6: Elution curves for unsaturated experiments

3.3 Desorption-only model inputs

The model input parameters are R_f, to set sorption behavior, and α, to set dispersivity. For each simulation, the R_f and α parameters were taken directly from the saturated experiment (R_f reported in Table 2). R_f was calculated from the area under the saturated elution curve, while α was adjusted until the curvature of the model elution curve aligned with the experimental curve.

3.4 Fluorescein

Figure 7 shows the results for saturated and unsaturated fluorescein experiments. The saturated experiment produced an elution curve consistent with the desorption-only model (Fig. 7a). Fluorescein was assumed to be a conservative tracer, but results indicate a small non-zero level of adsorption because $R_f > 1$, a result that has been observed by others for fluorescein.[22]

Figure 7b compares the experimental and simulated elution curves for unsaturated fluorescein. The desorption-only model predicts much higher outlet concentrations and quicker removal from the column. This difference can be quantified by the centroid of both elution curves. The desorption-only model centroid is 0.12 PV, while the experimental centroid is 1.22 PV. The difference is due to the tailing evident in the experimental elution curve, but not captured by the model curve. (Note that fluorescein did not reach a zero effluent concentration until approx. 10 PV.)

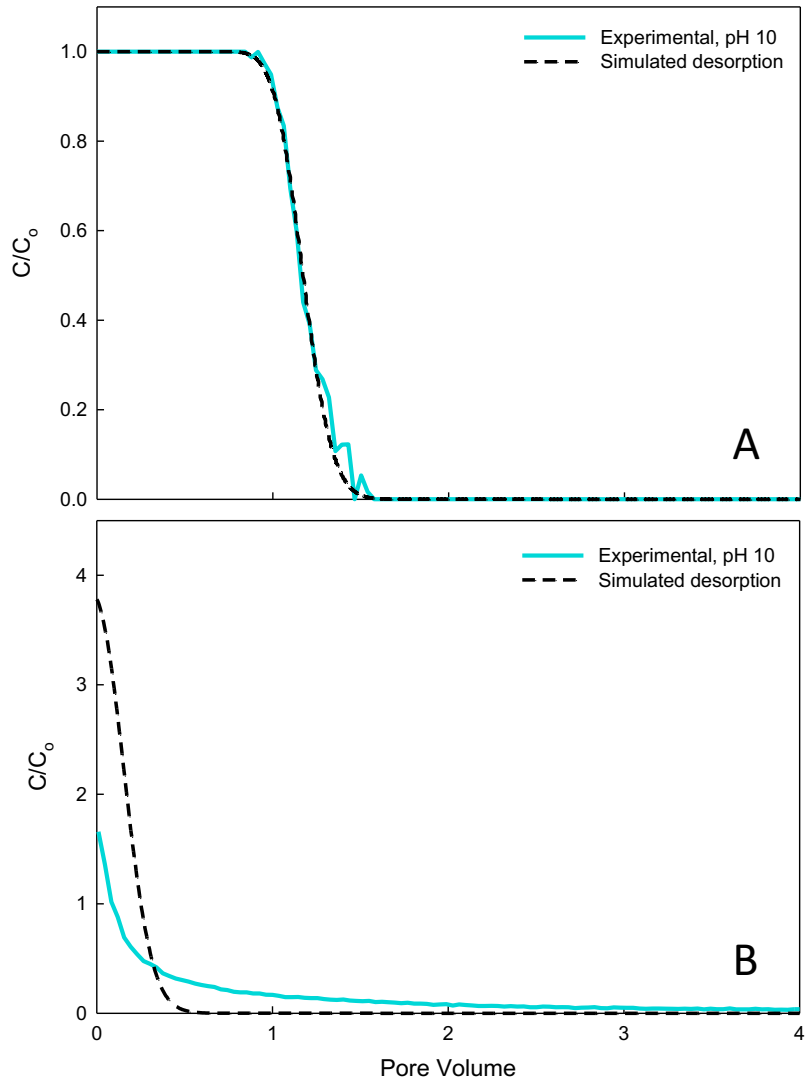


Figure 7: Fluorescein elution curves for a) saturated and b) unsaturated experiments. Dotted line simulates the desorption-only result.

3.5 Sulforhodamine B

Figure 8 shows the results for saturated and unsaturated sulforhodamine B experiments. The saturated experiment produced a curve similar to the desorption-only model (Fig. 8a). As with fluorescein, sulforhodamine B was assumed to be a conservative tracer, but an experimental $R_f > 1$ indicates some adsorption.

Figure 8b compares the experimental and simulated curves for unsaturated sulforhodamine B. As was the case with fluorescein (Fig. 7b), the model predicts a higher outlet concentration and quicker removal from the column than was observed. The simulation centroid is 0.20 PV, while the observed centroid is 1.05 PV. Thus the experimental data shows slower removal than the desorption-only model. Similar to fluorescein, this elution curve shows long tailing of concentration, contributing to the larger centroid value. (Note that sulforhodamine B did not reach a zero effluent concentration until approx. 11 PV.)

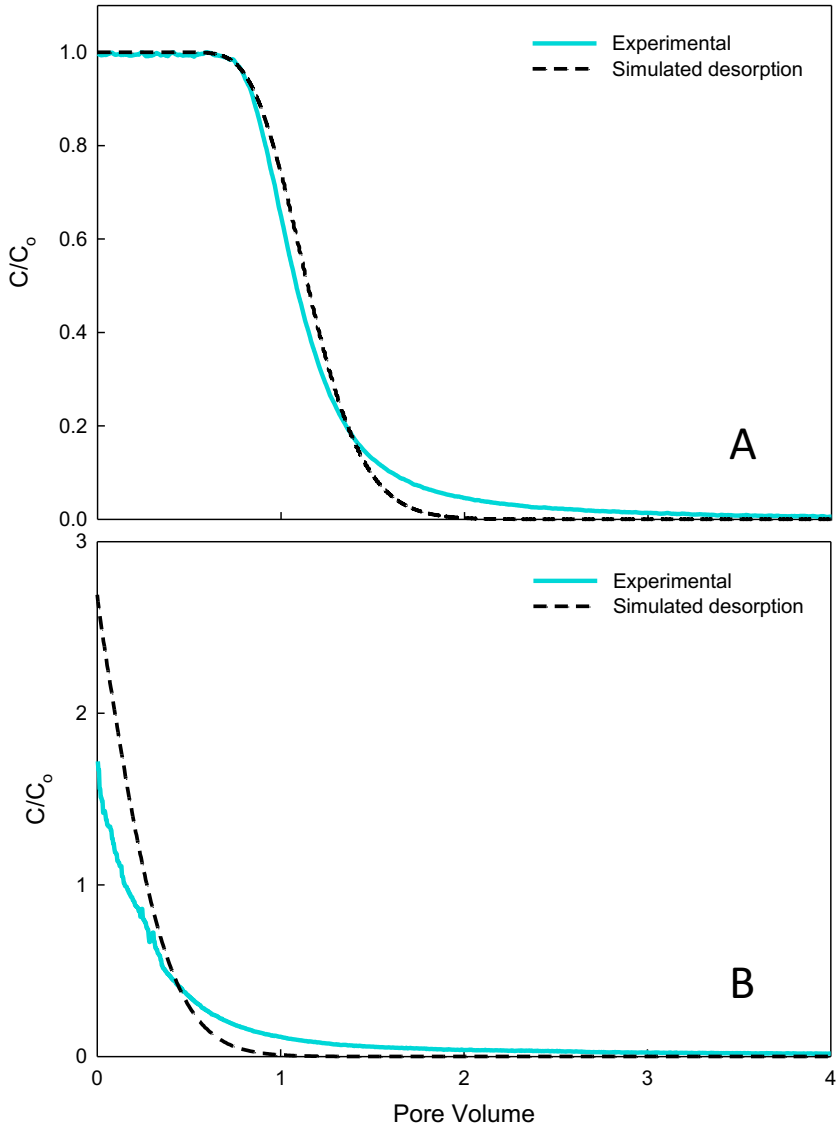


Figure 8: Sulforhodamine B elution curves for a) saturated and b) unsaturated experiments. Dotted line simulates the desorption-only result.

3.6 Caffeine

Figure 9 shows the results for saturated and unsaturated caffeine (pH 10) experiments. The experimental result is consistent with the desorption-only model, thus confirming the saturated transport model (Fig. 9a).

Figure 9b compares the experimental and simulated unsaturated curves for caffeine. The desorption-only model predicts a fast removal of caffeine, while the experimental data show bumps in the elution curve, and slower removal. The simulation centroid is 0.17 PV, while the observed centroid is 0.54 PV. Thus, the experimental data shows slower removal than the desorption-only model, a likely indication that the dynamics of dissolution are important in this system. Interestingly, unlike fluorescein and sulforhodamine B, the caffeine data do not exhibit long term tailing.

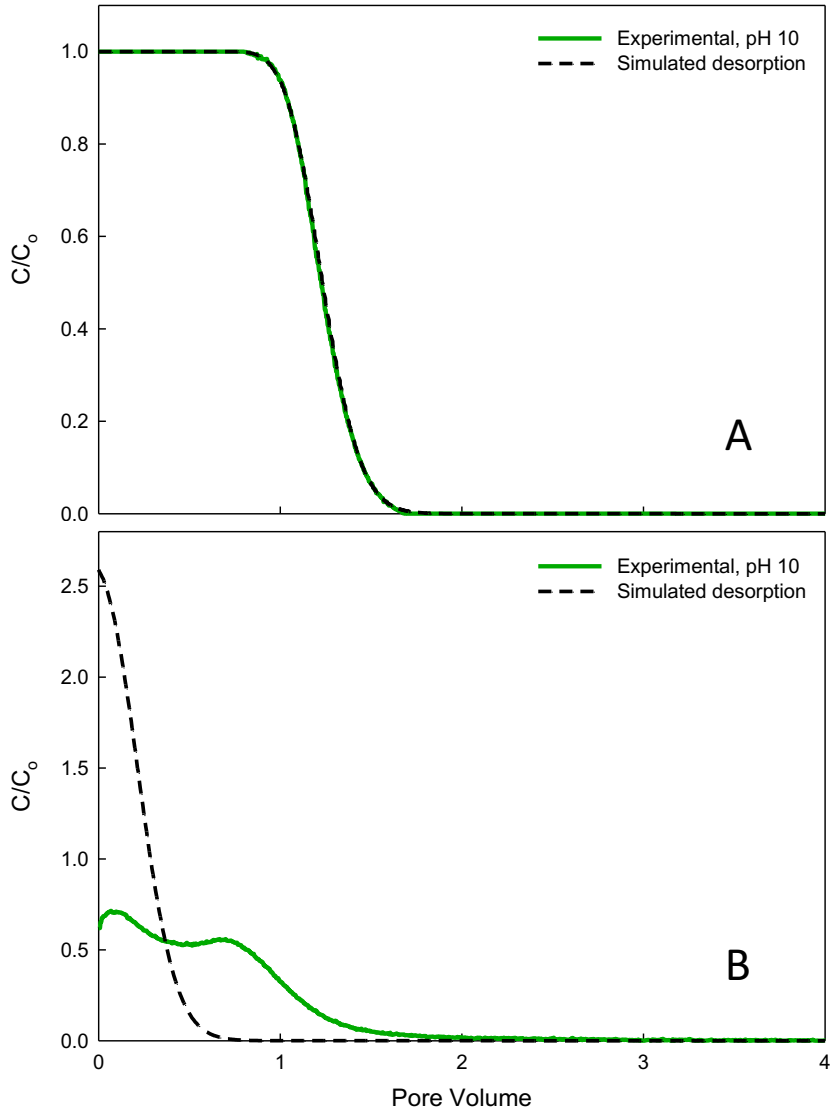


Figure 9: Caffeine elution curves for a) saturated and b) unsaturated experiments. Dotted line simulates the desorption-only result.

3.7 Propranolol

Figure 10 shows the results for saturated and unsaturated propranolol (pH 5, 10) experiments. For both pH values, the experimental result is consistent with the desorption-only model, thus confirming that the saturated transport model accounts for different pH conditions (Fig. 10a). Based on these curves, adsorption for pH > pK_a is much lower than for pH < pK_a. This indicates that propranolol adsorption is pH-

dependent about the $pK_a = 9.53$. For $pH < pK_a$, propranolol is positively charged and sand is negatively charged, allowing strong adsorption via electrostatic attraction. For $pH > pK_a$, propranolol is neutral, and sand is negatively charged, so little adsorption occurs.

Figure 10b compares the experimental and simulated curves for unsaturated propranolol at pH 5 and 10. For both pH conditions, the desorption-only model inaccurately predicts a faster removal of propranolol than is observed. Visually, the model looks to better predict the pH 10 behavior than the pH 5 behavior. For pH 5, the model and experiment centroids are 0.40 PV and 0.79 PV. For pH 10, the model and experiment centroids are 0.19 PV and 0.34 PV. These differences between experimental and model centroid values can be attributed to the effect of dissolution.

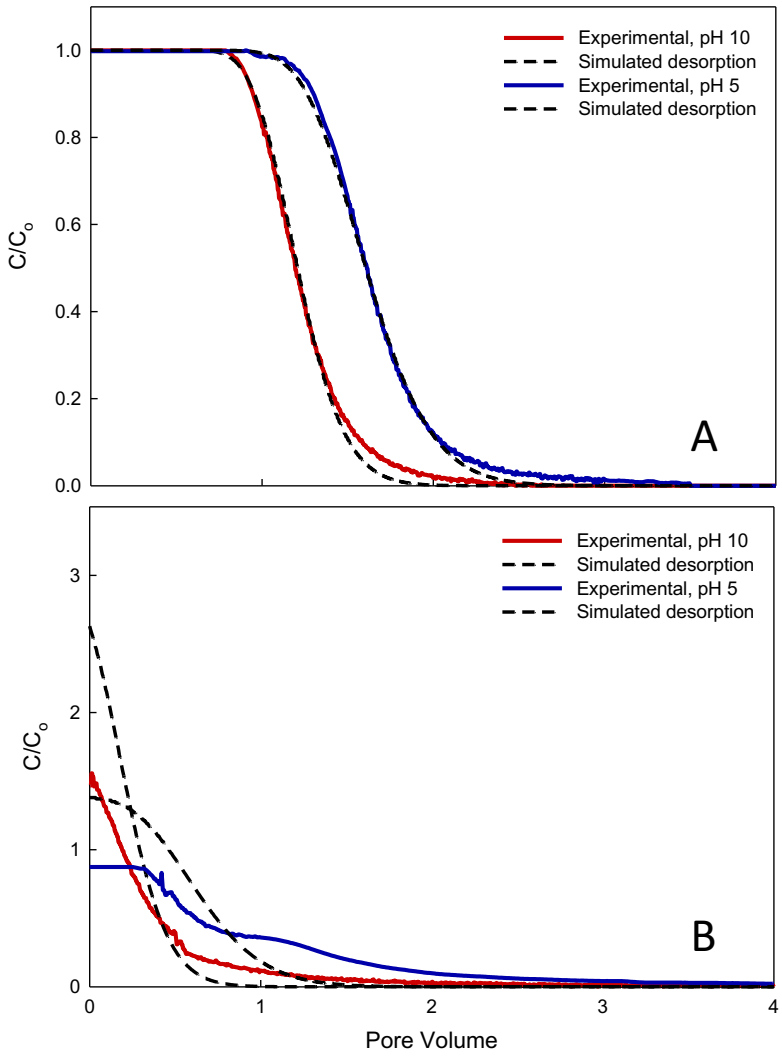


Figure 10: Propranolol elution curves for a) saturated and b) unsaturated experiments at pH 5 and 10. Dotted line simulates the desorption-only result.

3.8 Ciprofloxacin

Figure 11 shows the results for saturated and unsaturated ciprofloxacin (pH 3, 10) experiments. For both pH values, the saturated experimental result is consistent with the desorption-only model, with slight deviation for pH 3 results (Fig. 11a). The adsorption behavior is vastly dependent on pH, specifically regarding the proximity to the dissociation constants (pK_{a1} = 6.16, pK_{a2} = 8.62). Adsorption for pH < pK_{a1} is very

high because ciprofloxacin is primarily the positively charged species, and sand is negatively charged, allowing strong electrostatic attraction. For $pK_{a1} < pH < pK_{a2}$, ciprofloxacin is the neutral and zwitterionic species (zwitterionic meaning the overall charge is zero, but there is a negative charge and positive charge at different locations on the molecule), and the sand is negatively charged, so some adsorption occurs via cation exchange adsorption.[28] Finally, for $pH > pK_{a2}$, ciprofloxacin and the sand are negatively charged, preventing adsorption via strong electrostatic repulsion. Thus, the high adsorption of pH 3 ciprofloxacin yields an R_f of 11.122, which is an order of magnitude higher than any other compound/pH condition tested.

Figure 11b compares the experimental and simulated curves for unsaturated ciprofloxacin at pH 3 and 10. For pH 10, the model predicts, as in other cases, faster removal than observed. For pH 3 however, the model predicts that the high adsorption will cause the elution curve to have steady concentration during removal, and drop off gradually. This is not what is observed. In this case at pH 3, the actual curve rapidly decreases and tails, displaying the largest deviation of an experiment from a predicted elution curve. Similar to propranolol, visually, the model better predicts the high pH behavior than the low pH behavior. The centroids are used to compare the model and experiment curves. For pH 10, the model and experiment centroids are 0.28 PV and 0.49 PV. For pH 3, the model and experiment centroids are 5.2 PV and 23.4 PV. These differences can be attributed to the effect of dissolution.

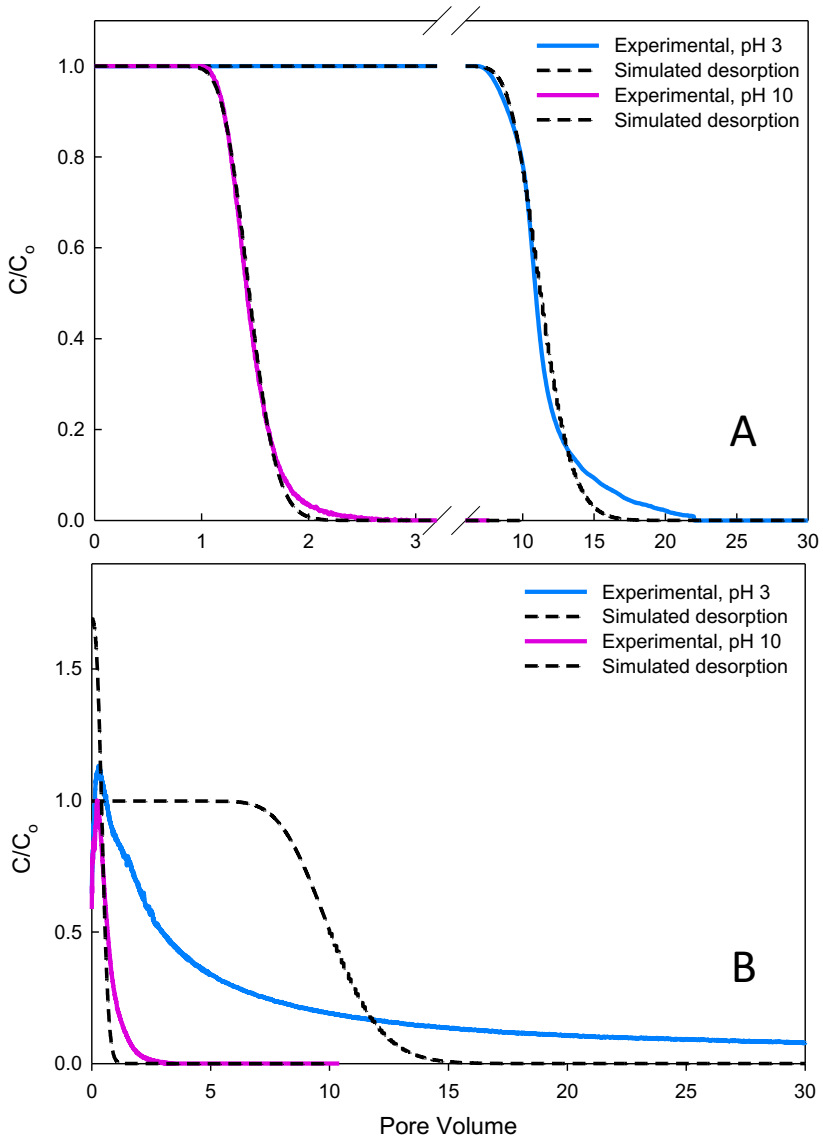


Figure 11: Ciprofloxacin elution curves for a) saturated and b) unsaturated experiments at pH 3 and 10. Dotted line simulates the desorption-only result.

3.9 Elution curve centroid analysis

Table 3 presents the centroid values for the unsaturated experimental and model elution curves and their ratio (X_{EXP}/X_{MOD}). The X-centroids for the desorption-only model (X_{MOD}) are smaller than the experimental X-centroids (X_{EXP}), yielding a ratio greater than 1 in every case. An X_{MOD} value smaller than X_{EXP} means that the centroid

occurs earlier (smaller PV) than the experimental data show. The difference between the centroids is interpreted as the effect of dissolution on removal. Fluorescein and sulforhodamine B have the two highest ratios, due to tailing in the unsaturated breakthrough curves that causes high X_{EXP} values (Figs. 7b, 8b). Since they are relatively conservative, the model predicts an early centroid (lower PV) because it does not predict this tailing. On the other hand, propranolol and ciprofloxacin (pH 10) have ratios closer to 1. These compounds had unsaturated elution curves with less tailing (Figs. 10b, 11b), so the model more closely duplicates the observed behavior.

Table 3: Elution curve centroids for experimental and model results

Compound	pH	Experimental X_{EXP} (PV)	Model X_{MOD} (PV)	Ratio X_{EXP}/X_{MOD}
Fluorescein	10	1.22	0.12	10.17
Sulforhodamine B	3	1.05	0.20	5.25
Caffeine	10	0.54	0.17	3.18
Propranolol	5	0.79	0.40	1.98
	10	0.34	0.19	1.79
Ciprofloxacin	3	23.4	5.2	4.50
	10	0.49	0.28	1.75

Figure 12 shows the relationship between the ratio of centroids and the concentration normalized to the compound solubility. In this plot, a higher X_{EXP}/X_{MOD} ratio means a higher effect of dissolution on the unsaturated elution curve, which causes slower removal from the column. Conversely, a ratio closer to 1 means that the X_{EXP} and X_{MOD} centroids are closer, and the dissolution effect is not significant compared to desorption (as described by the desorption-only model). The trend in the plot suggests

that experiments using a concentration much less than the solubility (i.e., $C_O \ll S$ and thus $C_O/S \ll 1$), will experience a higher effect due to dissolution. Consequently, the trend suggests that experiments using a concentration close to the solubility (i.e., $C_O \cong S$ and $C_O/S \cong 1$), will experience a lower effect due to dissolution.

Figure 13 shows the relationship between the ratio of the centroids and the distribution coefficient determined experimentally for each compound. There is no discernable trend in this data. A trend of some kind could suggest that the dissolution effect is somehow related to the adsorption (or hydrophobicity) of a compound, however the data do not support this.

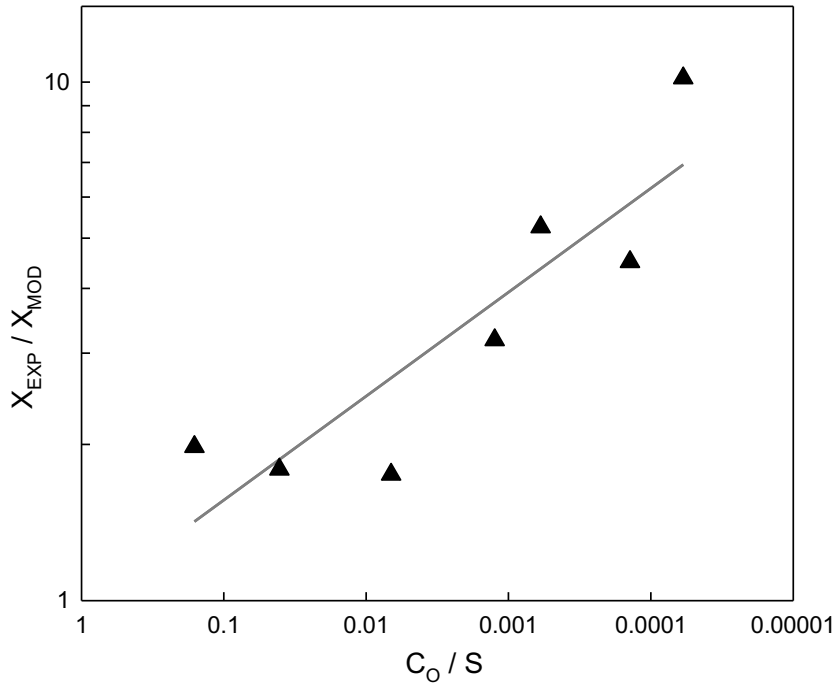


Figure 12: The relationship between the centroid ratio (X_{EXP}/X_{MOD}) and the concentration normalized to the compound solubility (C_O/S), on log-log scale.

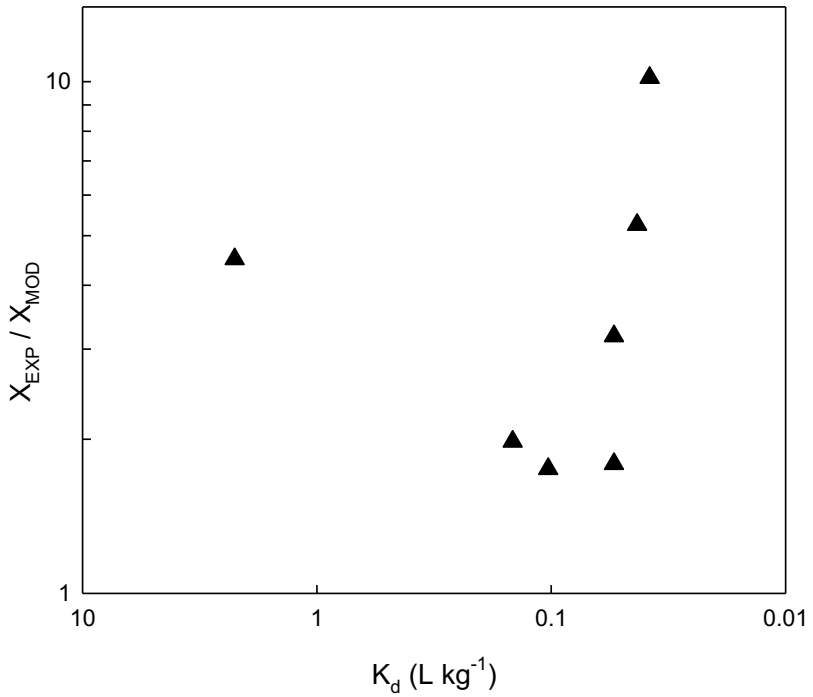


Figure 13: The relationship between the centroid ratio (X_{EXP}/X_{MOD}) and the experimentally-determined distribution coefficient (K_d), on log-log scale.

3.10 Discussion

The compounds and pH conditions explored here were selected to cover a wide range of adsorption behavior. From the near-conservative tracers to the highly adsorbing ciprofloxacin at pH 3, the desorption-only model consistently predicted faster removal from the sand column during flushing after evaporation than was observed. In reality, the data show lower initial outlet concentrations, curves that are less steep, and more time required for flushing out mass. A direct interpretation of these differences is that a process that is absent from the desorption-only simulation (e.g., dissolution) affects the elution curves by slowing down the removal of mass during flushing.

By using centroids, this analysis found that effect of dissolution was related to the concentration and solubility of the compound (Fig.12), and not the hydrophobicity

or adsorption behavior (Fig. 13). Comparing the centroid ratio (a measure of the effect of dissolution) to K_d and R_f values did not produce any trends, so it is concluded that the hydrophobicity and adsorption behavior have little effect on the unsaturated transport of compounds explored in this paper.

The trend explored found that as the initial concentration used approaches the solubility, the lower the effect of dissolution on removal during the sand column experiment. From the data available, some conclusions can be drawn. First, that compounds with very high solubility will experience dissolution effects during flushing if the inlet concentration (C_O) is chosen to be very low compared to its solubility. Second, that compounds with concentrations near their solubilities will experience less dissolution effects. One theory to explain this conclusion has to do with how C_O/S changes during evaporation. Compare the two scenarios: A) inlet concentration chosen such that C_O/S is close to 1, and B) inlet concentration chosen such that C_O/S is much less than 1. As both scenarios dry at the same rate, A will precipitate first, because its concentration began closer to the solubility initially. B will precipitate later, once its concentration exceeds its solubility. Following this theory, the earlier solid precipitate will experience fewer dissolution effects, likely due to differences in the configurations of precipitated solid. Additional pore level studies are needed to understand the physical differences between the systems that produce the observed behaviors.

3.11 Solid precipitate analysis

Table 4 shows the calculated molecular footprint following evaporation of the systems studied in this work. From the table, it can be seen that the area per molecule of all of the compounds is on the order of one molecule per nm^2, with a lower value

(0.025 mol nm^{-2}) observed for the fluorescein, and a higher value (4.458 mol nm^{-2}) for the strongly adsorbing pH 3 ciprofloxacin. These values are calculated based on a solid surface area of 198.28 cm^2 cm^{-3}, determined from sieve analysis, and assume a uniform coating on all solid surfaces. The magnitudes of the values in Table 4 are consistent with monolayer or sub-monolayer coverage. However, it is likely that coverage is non-uniform both on the solid surfaces and in the porous medium, as a result of the way solutes become concentrated and precipitate as the water evaporates. Regardless, this calculation suggests that interactions between individual molecules and the solid surface are likely to play an important role in the dissolution and remobilization that accompanies flushing.

Table 4: Molecular coating depth

Compound	Molecules (adsorbed)	Molecules (in solution)	Total Molecules/Area (mole. nm^{-2})
Fluorescein	1.01×10^{15}	2.36×10^{15}	0.025
Sulforhodamine B	2.00×10^{16}	4.12×10^{16}	0.459
Caffeine	5.07×10^{16}	8.32×10^{16}	1.005
Propranolol pH 5	3.80×10^{16}	2.31×10^{16}	0.459
Propranolol pH 10	1.41×10^{16}	2.31×10^{16}	0.279
Ciprofloxacin pH 3	5.71×10^{17}	2.26×10^{16}	4.458
Ciprofloxacin pH 10	2.16×10^{16}	1.86×10^{16}	0.302

3.12 Further exploration of dissolution effect

Further work was done to investigate the trend of increasing dissolution effect with a decrease in C_O/S ratio (Fig. 12). Figure 14 shows the results of the additional

unsaturated experiments with sulforhodamine B. These experiments were conducted in order to test the dissolution effect over a range of C_O/S values by choosing C_O = 4.16, 15, 41.6 and 150 mg L^{-1}. Based on the preliminary experiments conducted for the dye, the relationship observed in Fig. 12 is also followed in Fig. 14. This helps confirm that the trend is followed for each compound, and that the effect is not a result of the identity of the compound used.

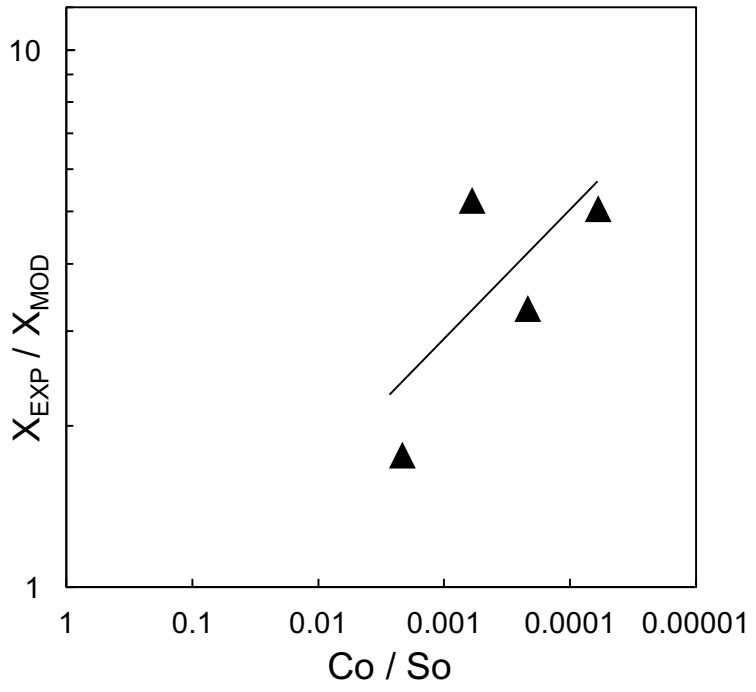


Figure 14: The relationship between the centroid ratio (X_{EXP}/X_{MOD}) and the concentration normalized to the compound solubility (C_O/S), on log-log scale, for additional sulforhodamine B experiments.

Chapter 4. Environmental Implications

This work has implications for understanding transport of contaminants in the environment. First, the transport in saturated and unsaturated experiments shows a large difference in behavior; the unsaturated experiments showed higher peak concentrations and more tailing than completely saturated experiments. This implies that across the compounds, the presence of an evaporation step affects the transport. In the natural environment, subsurface regions near the surface are prone to evaporation from seasonal heat and rapid imbibition during rain and flash-flooding. A contaminated subsurface region will therefore retain the contaminant differently based on the saturation conditions caused by drying and imbibition. A first implication of this work is that a completely saturated subsurface will produce expected transport of a contaminant, while conditions of varying saturation (drying, flooding) may produce higher peak discharge concentrations at first, with long tailing over time. Under some conditions, it is possible for contaminants released to have significantly higher concentrations than the concentrations present prior to evaporation.

A second implication of this work is that the transport behavior is also dependent on the given concentration and solubility of a compound. For the compounds examined here, the fluorescent dyes showed more dissolution effect than the pharmaceuticals, based on the centroid ratio. This is thought to be due to the distance between the chosen C_O and the compound's solubility. For C_O much lower than S, the dissolution effects are much higher than for C_O and S closer in value. This implies that for pharmaceuticals, the lower the concentration, the higher the dissolution effect. This has larger impacts for understanding transport in the unsaturated conditions

found in the environment, including that lower concentrations will be flushed from a dried region more slowly with excess tailing. Additionally, that higher concentrations (close to solubility), will be flushed from a dried region with little effect on removal due to dissolution.

References

1. Lapworth, D. J.; Baran, N.; Stuart, M. E.; Ward, R. S., Emerging organic contaminants in groundwater: A review of sources, fate and occurrence. *Environ Pollut* **2012,** *163*, 287-303.

2. Foolad, M.; Tran, N. H.; Jiangyong, H., Mobility and sorption of sewage chemical indicators onto tropical soils. In *Asian Conference in Civil, Material and Environmental Science*, Osaka, Japan, 2013; pp 602-606.

3. Li, W. C., Occurrence, sources, and fate of pharmaceuticals in aquatic environment and soil. *Environ Pollut* **2014,** *187*, 193-201.

4. Stackelberg, P. E.; Furlong, E. T.; Meyer, M. T.; Zaugg, S. D.; Henderson, A. K.; Reissman, D. B., Persistence of pharmaceutical compounds and other organic wastewater contaminants in a conventional drinking-water-treatment plant. *Sci Total Environ* **2004,** *329*, (1-3), 99-113.

5. Sui, Q.; Huang, J.; Deng, S.; Yu, G.; Fan, Q., Occurrence and removal of pharmaceuticals, caffeine and DEET in wastewater treatment plants of Beijing, China. *Water Res* **2010,** *44*, (2), 417-26.

6. Karnjanapiboonwong, A.; Morse, A. N.; Maul, J. D.; Anderson, T. A., Sorption of estrogens, triclosan, and caffeine in a sandy loam and a silt loam soil. *J Soils Sediments* **2010,** *10*, 1300-1307.

7. Zhou, J.; Broodbank, N., Sediment-water interactions of pharmaceutical residues in the river environment. *Water Res* **2014,** *48*, 61-70.

8. Focazio, M. J.; Kolpin, D. W.; Barnes, K. K.; Furlong, E. T.; Meyer, M. T.; Zaugg, S. D.; Barber, L. B.; Thurman, M. E., A national reconnaissance for pharmaceuticals and other organic wastewater contaminants in the United States--II) untreated drinking water sources. *Sci Total Environ* **2008,** *402*, (2-3), 201-16.

9. Kolpin, D. W.; Skopec, M.; Meyer, M. T.; Furlong, E. T.; Zaugg, S. D., Urban contribution of pharmaceuticals and other organic wastewater contaminants to streams during differing flow conditions. *Sci Total Environ* **2004,** *328*, (1-3), 119-30.

10. Fatta-Kassinos, D.; Hapeshi, E.; Achilleos, A.; Meric, S.; Gros, M.; Petrovic, M.; Barcelo, D., Existence of Pharmaceutical Compounds in Tertiary Treated Urban Wastewater that is Utilized for Reuse Applications. *Water Resour Manage* **2011,** *25*, 1183-1193.

11. Padhye, L. P.; Yao, H.; Kung'u, F. T.; Huang, C. H., Year-long evaluation on the occurrence and fate of pharmaceuticals, personal care products, and endocrine

disrupting chemicals in an urban drinking water treatment plant. *Water Res* **2014,** *51*, 266-76.

12. Liu, Z.; Sun, P.; Pavlostathis, S. G.; Zhou, X.; Zhang, Y., Adsorption, inhibition, and biotransformation of ciprofloxacin under aerobic conditions. *Bioresour Technol* **2013,** *144*, 644-51.

13. Subbiah, M.; Mitchell, S. M.; Ullman, J. L.; Call, D. R., beta-lactams and florfenicol antibiotics remain bioactive in soils while ciprofloxacin, neomycin, and tetracycline are neutralized. *Appl Environ Microbiol* **2011,** *77*, (20), 7255-60.

14. Laville, N.; Ait-Aissa, S.; Gomez, E.; Casellas, C.; Porcher, J. M., Effects of human pharmaceuticals on cytotoxicity, EROD activity and ROS production in fish hepatocytes. *Toxicology* **2004,** *196*, (1-2), 41-55.

15. Rizzo, L.; Fiorentino, A.; Grassi, M.; Attanasio, D.; Guida, M., Advanced treatment of urban wastewater by sand filtration and graphene adsorption for wastewater reuse: Effect on a mixture of pharmaceuticals and toxicity. *J Environ Chem Eng* **2015,** *3*, 122-128.

16. Lachassagne, D.; Soubrand, M.; Casellas, M.; Gonzalez-Ospina, A.; Dagot, C., Impact of sludge stabilization processes and sludge origin (urban or hospital) on the mobility of pharmaceutical compounds following sludge landspreading in laboratory soil-column experiments. *Environ Sci Pollut Res Int* **2015,** *22*, (21), 17135-50.

17. Zhang, D.; Gersberg, R. M.; Ng, W. J.; Tan, S. K., Removal of pharmaceuticals and personal care products in aquatic plant-based systems: a review. *Environ Pollut* **2014,** *184*, 620-39.

18. Henzler, A. F.; Greskowiak, J.; Massmann, G., Modeling the fate of organic micropollutants during river bank filtration (Berlin, Germany). *J Contam Hydrol* **2014,** *156*, 78-92.

19. Bradley, P. M.; Barber, L. B.; Duris, J. W.; Foreman, W. T.; Furlong, E. T.; Hubbard, L. E.; Hutchinson, K. J.; Keefe, S. H.; Kolpin, D. W., Riverbank filtration potential of pharmaceuticals in a wastewater-impacted stream. *Environ Pollut* **2014,** *193*, 173-80.

20. Bertelkamp, C.; Reungoat, J.; Cornelissen, E. R.; Singhal, N.; Reynisson, J.; Cabo, A. J.; van der Hoek, J. P.; Verliefde, A. R., Sorption and biodegradation of organic micropollutants during river bank filtration: a laboratory column study. *Water Res* **2014,** *52*, 231-41.

21. Chen, H.; Gao, B.; Li, H.; Ma, L. Q., Effects of pH and ionic strength on sulfamethoxazole and ciprofloxacin transport in saturated porous media. *J Contam Hydrol* **2011,** *126*, (1-2), 29-36.

22. Kasnavia, T.; Vu, D.; Sabatini, D. A., Fluorescent Dye and Media Properties Affecting Sorption and Tracer Selection. *Ground Water* **1999,** *37*, (3), 376-381.

23. Sabatini, D. A.; Austin, T. A., Characteristics of Rhodamine WTand Fluorescein as Adsorbing Ground-Water Tracers. *Ground Water* **1991,** *29*, (3), 341-349.

24. Bergstrom, C. A.; Norinder, U.; Luthman, K.; Artursson, P., Experimental and computational screening models for prediction of aqueous drug solubility. *Pharm Res* **2002,** *19*, (2), 182-8.

25. Avdeef, A., *Absorption and drug development : solubility, permeability, and charge state*. Wiley-Interscience: Hoboken, N.J., 2003; p xxiv, 287 p.

26. Lapidus, L.; Amundson, N. R., Mathematics of Adsorption in Beds. VI. The Effect of Longitudinal Diffusion in Ion Exchange and Chromatographic Columns. *J Phys Chem* **1952,** *56*, (8), 984-988.

27. Chen, L.; Kibbey, T. C., Measurement of air-water interfacial area for multiple hysteretic drainage curves in an unsaturated fine sand. *Langmuir* **2006,** *22*, (16), 6874-80.

28. Xu, X.; He, H.; Li, Y.; Fang, Z.; Xu, S., Adsorption and Transport of Ciprofloxacin in Quartz Sand at Different pH and Ionic Strength. *Open Journal of Soil Science* **2014,** *4*, 407-416.